An adjoint body-force approach for fully-coupled aero-propulsive optimizations

Cyril Dosne, Raphaël Barrier, Sébastien Bourasseau, Marco Carini, Rocco Moretti, Jacques Peter

EUROGEN 2023
15th ECCOMAS Thematic Conference on
Evolutionary and Deterministic Methods for Design, Optimization and Control
N. Gauger, K. Giannakoglou, M. Papadrakakis, J. Periaux (eds.)
Chania, Crete Greece, 1–3 June 2023

AN ADJOINT BODY-FORCE APPROACH FOR FULLY-COUPLED AERO-PROPULSIVE OPTIMIZATIONS

C. Dosne[1,3], R. Barrier[1], S. Bourasseau[2], M. Carini[1], R. Moretti[1] and J. Peter[2]

[1] DAAA, ONERA, Université Paris Saclay
F-92190 Meudon - France
e-mail: {cyril.dosne, raphael.barrier, marco.carini, rocco.moretti}@onera.fr

[2] DAAA, ONERA, Université Paris Saclay
F-92322 Châtillon - France
e-mail: {sebastien.bourasseau, jacques.peter}@onera.fr

[3] Institut Polytechnique de Paris
F-91120 Palaiseau - France

Keywords: adjoint method, body-force, aerodynamic, propulsion, optimization

Abstract. *Innovative aircraft studies often involve disruptive engine integration concepts, such as distributed propulsion, boundary-layer ingestion or unducted fan strongly interacting with the airframe. For such designs, airframe-engine aerodynamic interaction must be taken into account starting from the early design phase, with the need for computational-effective and reliable approaches to support a large number of design iterations and preliminary optimizations. Body-Force Modeling (BFM) methods have successfully allowed a faithful reproduction of the engine performance trends for analysis and design studies, while significantly reducing the simulation time and memory costs. However, an adjoint formulation is mandatory to efficiently use such models in gradient-based optimization involving a large number of airframe and engine shape parameters at once. Thus, a discrete Adjoint formulation based on explicit Body-Force Modeling (ABFM) is proposed to tackle highly coupled aero-propulsive optimization for preliminary design. The methodology is illustrated here using a simplified body-force model to optimize a 2D Distributed Propulsion (DP) configuration, involving both lumped engine parameters and airfoil shape design variables at the same time. The contribution of the ABFM to the adjoint solution and to the shape gradients is analysed, showing an important influence on both. Preliminary optimisation results are then presented.*

1 INTRODUCTION

Environmental challenges urge the aeronautic sector to decrease the air traffic carbon footprint by 50% in 2050 relative to 2005 levels [1, 2, 3]. Over the past decades, the conventional aircraft configurations have been optimized while minimizing the aerodynamic interactions between the airframe and the engines, integrating them under the wings or on the fuselage side. However, such design paradigms seem to have reached an asymptotic efficiency [4]. For instance, a further increase of the By-Pass Ratio (BPR) would raise structural and operational issues, as at max climb and cross-wind conditions the interaction between the fan aerodynamic and the airframe can no longer be neglected [5, 6]. Thus, new aircraft configurations exploiting aero-propulsive synergies are investigated [7, 8, 9]. The forthcoming introduction of ultra high by-pass ratio engines as well as the increasing attention towards new engine integration architectures, such as distributed propulsion or boundary-layer ingestion for instance, require a coupled modeling of the aerodynamics and propulsion sub-systems. Indeed, for such innovative configurations, a coupled design approach is essential to correctly predict their performance and thus maximize the aero-propulsive gains.

In the past years, several studies on high-fidelity multidisciplinary optimization have focused on aero-structure design, showing relevant potential improvements for the next generation of aircrafts with increased flexibility [10, 11]. However, only few optimization studies have been dedicated to aero-propulsive architectures by means of a coupled approach. Several studies have been conducted on the distorted engine inlet conditions and the minimization of their influence on the engine performance to obtain an optimized fan design. Most of them used the adjoint methodology to compute the sensitivities of the distortion metrics regarding the engine inlet shape [12, 13, 14]. In addition, propulsive models were used to ensure a reasonable optimization computational cost.

Indeed, simulating the engine aerodynamics under distorted inlet conditions using CFD would require a computational domain as large as one distortion pattern at least. Besides, considering a stationary azimuthal inlet distortion in the aircraft reference frame, the blade undergoes a periodic forcing during its rotation, and therefore an unsteady simulation is required to reproduce the distortion transfer across the engine [5, 15, 6]. As an example, when considering engines buried in the airframe, complex and costly simulations - like URANS - are required to study the aero-propulsive synergies and assess the overall performances. However, such simulations are cost prohibitive for preliminary optimization studies, and would require advance adjoint capabilities - such as unsteady adjoint - to be integrated in a gradient-based optimization framework. Thus, lower fidelity propulsive models are necessary to study such innovative engine integration architectures. In a recent study, Kenway used the actuator zone model [12], that applies a given engine thrust in the fan-swept volume with no direct dependency on the local flow state. Ordaz and Gray [13, 14] both used outflow and inlet boundary conditions at the inlet and outlet fan-swept volume surfaces. These boundary conditions allowed them to simulate the enthalpy and entropy rises, using a 1D thermodynamic model. The fan pressure ratio and the mean static pressure at the fan face were considered to compute the total fan thrust. Thus, the engine lumped parameters - here the total thrust - depend only on the averaged flow state at the engine inlet boundary. Such models can be considered as weakly coupled to the flow equations, since no local information from the internal flow stream affects the engine performances. As a consequence, no distortion effects can be taken into account by such models, while this is key to the global aero-propulsive efficiency trade-off [16]. In their recent work, Gray *et al.* [8] modified their engine model to simulate the internal flow stream of a BLI configuration, using a

body-force methodology and considering the body-force applied on the engine flow as a design variable of the optimization. Therefore, the CFD aeropropulsive simulation is enriched and the forces applied on the engine internal surfaces can be accounted for. However, the fan thrust is still computed by a 1D thermodynamic model, relying on integral flow variables at the fan face, featuring a constant fan polytropic efficiency. Therefore, inlet distortions effects on the engine performances cannot be directly taken into account. The authors decided to add a constraint on the distortion metrics to control the distortion amplitude. However, the aero-propulsive trade-off misses information on the fan efficiency off-set due to inlet distortions.

On the other hand, in recent research studies, the body-force modeling methodology has proven its ability to properly reproduce the local blade work added to the flow and its associated efficiency [15], even under distorted conditions [5, 17, 18, 16]. It reproduces with a good accuracy the turbofan performance trends and capture the main aero-propulsive coupling effects, including the distortion transfer across the engine [18, 17, 5] at a computational cost two order of magnitude lower than the URANS [16].

Explicit body-force models rely analytically and directly on the local flow field W, the mesh coordinates X and the blade shape parameters β to compute the source terms. On the contrary, data-based body-force models rely on high-fidelity simulation data - using interpolations [17] or neural networks for instance [19] - to compute the source terms, and therefore the functional dependancy of S to W and β is not straightforward. Given their direct dependence on engine parameters, explicit models are naturally adapted to optimization problems. They are also found more robust than the data-based ones [6]. For instance, the Hall model [20], improved by Thollet [15], introduces a direct dependence on 'engineer' blade shape parameters, like the local blade chord or camber, making it suitable for optimization studies handling airframe and engine blade parameters at once. Such models have already been used to conduct parametric studies on both fan and nacelle geometries for short inlet high by-pass ratio engine designs [5, 6]. Then, they were also used to undertake the first rotor/stator blade shape optimizations under inlet distortions [20, 16]. All these studies have proven the BFM capacity to undertake complex trade-offs on highly coupled external-internal flow conditions. However, to the best of the authors' knowledge, no adjoint formulation of these models has been proposed so far in the literature. The lack of an efficient method to compute the gradients of the Quantities of Interest (QoI) with respect to the design parameters restricts the design space dimension that can be explored during the optimization at an affordable computational cost, when using these models. It also implies robustness issues in the optimization loop when using finite differences [16]. To efficiently integrate the BFM in a gradient-based optimization framework, an adjoint body-force is hence needed.

In this context, the goal of this paper is to present the adjoint body-force equations and the implementation methodology retained, and then to show the preliminary results obtained for a simplified body-force model used as a prototype. This new tool will enable us to capture the main coupling effects between the propulsion system and the external aerodynamics, by providing access to their sensitivities for different QoIs, like the fan power consumption. This implementation methodology features genericity and modularity and benefits from algorithmic differentiation softwares, making it suitable for any explicit body-force model.

The ABFM implementation strategy is first presented and the code structure validated using an analytic test case in section 2. Then, the ABFM methodology is applied to a simplified BFM model featuring lumped engine parameters in section 3. Using this simplified model and

its adjoint formulation, a first demonstration of the use of ABFM sensitivities in a gradient-based optimization framework is undertaken on a two-dimensional test case representative of a distributed propulsion design, in section 4. Finally the on-going developments and analysis will be discussed.

2 METHODOLOGY AND IMPLEMENTATION

2.1 Body-Force Modeling (BFM)

All BFM methods rely on reproducing the blade effect on the engine flow by adding source terms to the right hand side of the steady RANS equations. To do so, one must consider a single blade-to-blade row channel and circumferentially average the blade aerodynamic force applied to the fluid. The resulting equations can be used to build up a model relying on the local flow and the model parameters. As consequences, the source terms are purely local. According to the literature, a steady body-force computation provides a good approximation of the time-averaged engine flow and performances, for both rotor and stator blade rows [20, 15], even under inlet distortions [5, 6]. However, the fidelity of the currently available BFM models decreases when studying off-design operating points, if the model is not re-adapted for these conditions [15]. These source terms are expected to reproduce the enthalpy and entropy rise across any blade wheel, based on the local flow state W. The general formulation is summarized as follows:

$$R(X, W) - S = \tilde{R}(X, W, S) = 0\,, \tag{1}$$

where we denote by S the body-force source terms, R the residuals of the discretized RANS equations and $\tilde{R}$ their augmented form, i.e. including body-force contribution. As the forces applied to the flow are modeled for the whole engine row, its blades are not meshed. Therefore, the body-force mesh is far simpler and smaller in size than its blade-fitted counterpart, thus reducing the memory and CPU wallclock-time needed to undertake the simulation [16]. Furthermore, this methodology can simulate accurately an inlet distortion transfer across the engine stages [6].

Explicit body-force models intend to analytically evaluate the blade force applied to the fluid, based on the local flow variables W and the engine parameters β. These latter can include both engine global variables, like rotational speeds or its total thrust, as well as blade shape parameters. Consequently, the functional dependencies of the source terms can be expressed as $S = S(X, W, \beta)$. Considering the absence of a blade metal blockage modeling, neglecting any contribution to the one-equation turbulence model considered here, denoting $\overrightarrow{v}$ the local flow velocity vector in the absolute reference frame, ρ the local flow density and $\overrightarrow{f}$ the local BFM force applied to the fluid, the general expression of S reads :

$$S = \left\{ \begin{array}{l} S_\rho \\ \overrightarrow{S_{\rho\vec{v}}} \\ S_{\rho E} \\ S_{\tilde{\nu}} \end{array} \right\} = \left\{ \begin{array}{l} 0 \\ \rho\overrightarrow{f} \\ \rho\overrightarrow{f} \cdot \overrightarrow{v} \\ 0 \end{array} \right\} . \tag{2}$$

2.2 Adjoint Body-Force Modeling (ABFM) equations

Enhancing the aero-propulsive system performance through a simultaneous optimization of the airframe shape variables α and the engine parameters β requires to deal with a large number of design variables and a small number of functions of interest. Therefore, the adjoint methodology is of great interest to precisely and efficiently compute the associated gradients [21]. A discrete adjoint framework [22] is considered here since it enable to compute the sensitivities

of a QoI $\mathcal{J}(X, W)$, evaluated at the steady state solution $R(X, W) = 0$, with an accuracy that can reach the machine precision [23].

If the propulsive system is modelled using an explicit BFM model, the adjoint equations must be re-written to take into account the body-force contribution to the adjoint system and to the QoI gradients. As a QoI may directly depend on the body-force source term - $\mathcal{J} = \mathcal{J}(X, W, \beta)$ - its gradient with respect to the engine design parameters β, at residual convergence $\tilde{R}(X, W, S) = 0$, reads:

$$\frac{d\mathcal{J}}{d\beta} = \frac{\partial \mathcal{J}}{\partial X}\frac{dX}{d\beta} + \frac{\partial \mathcal{J}}{\partial W}\frac{dW}{d\beta} + \frac{\partial \mathcal{J}}{\partial \beta}\,, \tag{3}$$

$$\frac{d\tilde{R}}{d\beta} = \frac{\partial R}{\partial X}\frac{dX}{d\beta} + \frac{\partial R}{\partial W}\frac{dW}{d\beta} \underbrace{- \frac{\partial S}{\partial X}\frac{dX}{d\beta} - \frac{\partial S}{\partial W}\frac{dW}{d\beta} - \frac{\partial S}{\partial \beta}}_{\text{additional contributions due to the BFM source terms}} = 0\,. \tag{4}$$

Let us introduce the adjoint body-force equations, obtained using the methodology detailed in [21]:

$$\underbrace{\left(\frac{\partial R}{\partial W} - \frac{\partial S}{\partial W}\right)^T}_{\text{BFM contribution}} \tilde{\Lambda} = -\frac{\partial \mathcal{J}}{\partial W}\,. \tag{5}$$

where the term within brackets correspond to the Jacobian operator associated with the augmented residuals. Then, by multiplying eq. 4 by $\tilde{\Lambda}^T$, adding it to eq. 3 and substituting from eq. 5, we obtain the following gradient expression:

$$\frac{d\mathcal{J}}{d\beta} = \left(\frac{\partial \mathcal{J}}{\partial X} + \tilde{\Lambda}^T\frac{\partial \tilde{R}}{\partial X}\right)\frac{dX}{d\beta} + \underbrace{\left(\frac{\partial \mathcal{J}}{\partial \beta} + \tilde{\Lambda}^T\frac{\partial \tilde{R}}{\partial \beta}\right)}_{\text{BFM direct contribution to sensitivities}}\,. \tag{6}$$

The gradients of $\mathcal{J}$ with respect to the aerodynamic shape parameters α simply reduces to the usual expression:

$$\frac{d\mathcal{J}}{d\alpha} = \underbrace{\left(\frac{\partial \mathcal{J}}{\partial X} + \tilde{\Lambda}^T\frac{\partial \tilde{R}}{\partial X}\right)}_{\text{BFM indirect contribution}}\frac{dX}{d\alpha}\,, \tag{7}$$

as S does not depend on α. We can observe that, even considering the QoI sensitivities to α, the BFM still adds a contribution to the adjoint system. Therefore, the BFM indirectly contributes to the QoI sensitivities through the adjoint vector. This shows that the airframe and the engine aerodynamics are coupled even when evaluating the QoI gradients. Moreover, an additional contribution appears in the QoI gradient regarding the engine parameters β, as shown in eq. 6, corresponding to the direct sensitivities of the BFM model to β.

2.3 BFM and ABFM implementation aspects

As previously shown in eq. 2, body-force source terms are all built upon a generic structure. Besides, by analyzing Thollet's [15] investigation and enhancement of existing explicit BFM models, we observe that most of them define the blade force $\overrightarrow{f}$ as a function of the local flow variables projected in the local blade skeleton coordinate system. Therefore, most of the operations required to compute S from W are common between those various models. In addition, the enhancements proposed by Thollet - such as the quadratic losses estimation or the Prandtl-Ackeret compressibility correction - can be applied to any of the studied models. Similarly, the blade metal blockage modelisation proposed by Kottapalli [24] is independent from the chosen model. Finally, body-force models are expected to evolve to better capture the engine aerodynamics. Therefore, a generic and modular implementation of the BFM seems preferable to reduce the implementation and validation effort necessary for any new model. Each basic operation required to compute S from W would define a module, implemented and validated only once. Chaining these modules from their required inputs and outputs will lead to the desired explicit BFM model. Besides, considering the proven capacities of source transformation algorithmic differentiation engines like Tapenade [25], the adjoint formulation of each module can be obtain and validated easily from the primal implementation. With such code architecture, any new BFM model to implement will benefit from the existing ones in the code, and so will its adjoint formulation.

As schematized in figure 1, a modernized module [26] of the *elsA* software [27] (ONERA-SAFRAN property) has a code structure based on basic operators sharing the same attributes and methods thanks to the C^{++} Object-Oriented Programming capabilities. Operations affecting the data vectors are implemented in Fortran scripts for computation effectiveness, wrapped by the C^{++} operator, managing the HPC layer and the code execution. An automate automatically chains the operator from their inputs and outputs. The user can provide external operators to the CFD software to enable new computational capabilities. Therefore, such code structure allows for a proper modification of the CFD software to take into account BFM source terms, and provides the genericity and modularity structure researched in the previous paragraph. In addition, like some other *elsA* modules, this modernized part has adjoint capabilities. In the *elsA* software, the discrete adjoint implementation has been chosen [22], since it can provide the sensitivities of the functions of interest up to zero-machine precision [23]. Tapenade is used to produce both the tangent and adjoint codes from source transformation of the primal implementation, once validated. Thus, it has been decided to create an inhouse library called BACARDI, external to *elsA* and interfaced with its modernized module, implementing all body-force modules using the *elsA* operator structure, as depicted in figure 2.

The user interacts with the BACARDI library thanks to a python script, and build all the BFM operators corresponding to the chosen model. Then BACARDI automatically adds these operators to the *elsA* modernized module, which will then chain all CFD and BFM operators all togethers. Thus, the solver can solve the CFD problem integrating the BFM forcing. In the same way, when interfaced with BACARDI, the modernized CFD software can solve the ABFM adjoint equations given in eq. 5. However, the additional direct contribution of the ABFM to the QoI sensitivities with respect to the engine design variables cannot natively been computed by *elsA*. This capability must then be added to the CFD software.

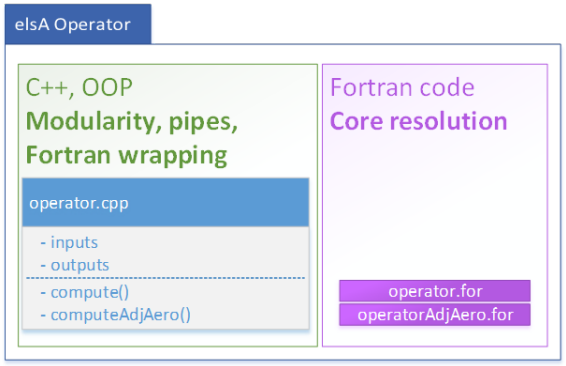

Figure 1: the modernized *elsA* module framework

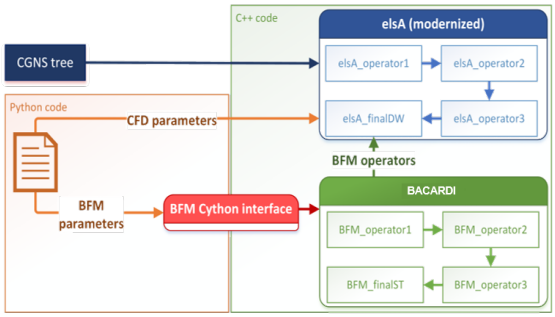

Figure 2: the BACARDI external library interfaced with the modernized *elsA* module, providing both BFM and ABFM capabilities

2.4 Code structure implementation and validation

In order to perform a first validation of the adjoint body-force implementation, we consider an academic test case for which the primal solution and the QoI gradients are analytically known. Such a model consists of the steady 1D-Euler supersonic flow of an ideal gas along a mono-dimensional channel of unitary length, starting from $x_0 = 0$ to $x_1 = 1\,\text{m}$. The BFM forcing is applied all along this channel. The flow is fully supersonic so all boundary parameters can be applied on the inlet. The solution is governed by the following equations :

$$\begin{cases} \dfrac{d\left(\rho u\right)}{dx} = 0 \\ \dfrac{d\left(\rho u^2 + P\right)}{dx} = \rho f \\ \dfrac{d\left(\rho u h_t\right)}{dx} = \rho u f \end{cases}, \tag{8}$$

where ρ is the flow density, u the flow velocity, P the static pressure and h_t the total enthalpy. We decide to enforce a linear velocity solution, governed by a body-force parameter β_{1D} :

$$u(x) = u_0\left[1 + \beta_{1D}\left(x - x_0\right)\right] \text{ with } \beta_{1D} = \frac{\frac{u_1}{u_0} - 1}{x_1 - x_0}. \tag{9}$$

Using the manufactured solution method, under isentropic flow asumption, the body-force forcing reads :

$$f = \beta_{1D}\left[u u_0 - c_0^2\left(\frac{u_0}{u}\right)^{\gamma}\right]. \tag{10}$$

where c_0 represents the speed of sound for the inlet flow conditions and γ is the heat capacity ratio of the air. The validation of the BFM implementation against the analytic results is shown in figure 3a.

The chosen objective function is defined as the total energy supplied by the volume force to the flow, integrated over the all body-force domain volume V_{BFM}, denoted $\mathcal{F}_{POW}$ and given by the general expression:

$$\mathcal{F}_{POW}(X, W, S) = -\iiint_{V_{BFM}} S_{\rho E}(\vec{f})dV\,. \tag{11}$$

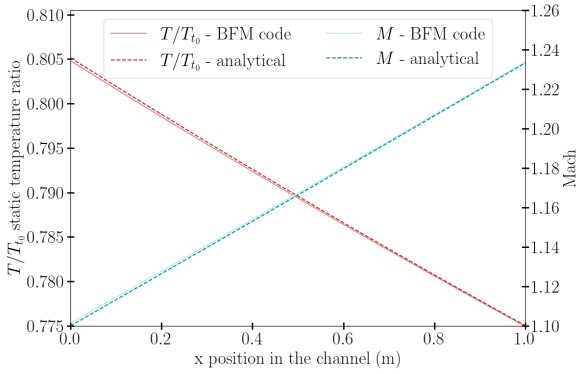

(a) Static temperature ratio (in orange), and Mach flow field (in blue) along the channel. Results obtained from the BFM code are plotted in plain lines, analytic values are plotted in dashed lines.

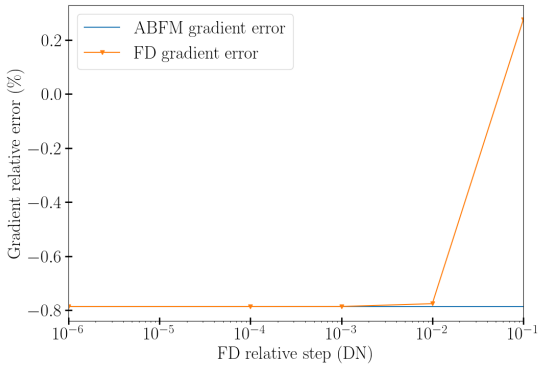

(b) ABFM gradient relative error with respect to analytic expectation. Comparison against FD gradients computed for several relative step size of β_{1D}.

Figure 3: BFM (left) and ABFM (right) validation for the analytic test case

In this monodimensional case, $\mathcal{F}_{POW}$ simplifies as follow:

$$\mathcal{F}_{POW}(u, \beta_{1D}\,;u_0, c_0) = -\int_{x_0}^{x_1} \rho u f dx\,. \tag{12}$$

Since ρu is constant along the channel, the analytic expression of $\mathcal{F}_{POW}$ can be obtained by substituing f for its expression given in eq. 10:

$$\mathcal{F}_{POW}(u, \beta_{1D}\,;u_0, c_0) = -\rho u \int_{x_0}^{x_1} f dx \tag{13}$$

$$= -\rho u \left(\frac{{u_1}^2 - {u_0}^2}{2} + \frac{{c_0}^2}{\gamma - 1}\left[\left(\frac{u_0}{u_1}\right)^{\gamma-1} - 1 \right] \right)\,. \tag{14}$$

As $\mathcal{F}_{POW}$ and u are analytically known, so is $\mathcal{F}_{POW}$ derivative with respect to β_{1D}:

$$\frac{d\mathcal{F}_{POW}}{d\beta_{1D}} = \rho u u_0 \cdot \frac{u_1 - u_0}{\beta_{1D}} \left[\frac{u_1}{u_0} - \left(\frac{c_0}{u_0}\right)^2 \left(\frac{u_1}{u_0}\right)^{-\gamma} \right]\,. \tag{15}$$

In our CFD computations performed with *elsA* we consider $M_0 = 1.1$, $T_{i_0} = 302.4\,K$ and $P_{i_0} = 120\,108.30\,Pa$ as supersonic inlet conditions. Convective flux are discretized using the Roe scheme, without limiter. The mesh is composed of one hundred cuboids along the x axis, and is treated as unstructured. In figure 3b, one can see the very good agreement between the ABFM-computed gradient and the gradient estimated by centered finite differences (FD) for various relative steps. Both gradients show a small residual offset from the analytic expectation, by $-0.8\,\%$.

These results ensure the BFM and ABFM implementation are valid, and thus the code architecture is correct. Therefore, the framework is ready for the implementation of BFM models of interest, of growing complexity and fidelity.

3 ABFM RESULTS ON A 2D TEST CASE

3.1 A Distributed Propulsion test case geometry featuring a simplified BFM model

A simplified body-force model has been implemented into the BACARDI library and then used on a 2D test case geometry modeling a distributed propulsion wing section, with a rear-mounted engine on the suction side. This BFM model, later called 'T-spread' in this paper, relies only on lumped engine parameters, which is useful at the conceptual design stage, for which no detailed engine design exists yet. This model provides a first proof of concept of adjoint body-force for coupled aero-propulsive optimizations. For such model, the analytic formulation of the force f of eq. 2 is based directly on :

- the local flow velocity in the absolute frame of reference $\overrightarrow{v}$,
- the total thrust provided by the engine T,
- the total sub-domain volume where the body-force model is active V_{BFM}

Thus, f reads :

$$\overrightarrow{f} = \frac{\overrightarrow{v}}{\rho \left\| \overrightarrow{v} \right\|} \cdot \frac{T}{V_{BFM}} \,. \tag{16}$$

The considered geometry, shown in figures 4 and 5a, consists of a NACA 23012 airfoil for the main wing section and a Clark-Y airfoil for the engine nacelle. As depicted in figure 4, the mesh is unstructured, and composed of prism layers around the airfoils to properly discretize the boundary layers, and of tetrahedra elsewhere. The mesh is composed of approximately $77 \cdot 10^3$ cells, and the computational domain size is 300 times the NACA chord length c_{NACA}. The first cell of the prism layers features a $2.4 \cdot 10^{-6} c_{\text{NACA}}$ height. Viscous wall boundary conditions are imposed at the airfoils skin, and non-reflective boundary conditions are imposed on the limit of the computational domain. One can see in figure 5b the total pressure-ratio rise across the propulsion system obtained by the BFM forcing, and in figure 5c a representation of the region where this forcing is active. As one can see in the latest, the BFM forcing is decreased near the NACA wall to avoid boundary-layer non-physical separation. These results have been obtained by a RANS simulation, taking into account the contribution of the body-force source terms in the flux balance. The negative Spalart-Allmaras turbulence model was used for this test case. The convective fluxes are discretized using the Roe scheme. The discrete viscous fluxes are computed based on cell-centered gradients corrected at the interface in the direction of the two adjacent centers. The considered flow conditions features a Reynolds number $Re = 1.165 \cdot 10^7$ and a Mach number $M = 0.2$.

The position of the Clark-Y nacelle can be modified by shifting it along the z axis trough the parameter τ_z, or rotating it around an axis parallel to the y-axis intersecting the profile at its trailing edge through the parameter θ_y. The size of the Clark-Y profile can be modified using the σ coefficient. Again, the Clark-Y profile position along the x-axis is anchored at the trailing edge, the scaling coefficient thus affects the position of the leading edge. On the NACA profile, only the suction side can be altered. This curve is parametrized by the CST method [28], using 16 coefficients to represent the curve. The 5 coefficients affecting mainly the rear of the suction side can be used as design variables. They are denoted Π_{v_1} from the trailing edge to Π_{v_5} and enable to modify the engine inlet diffuser. Since such parametrization would modify the volume of the body-force zone, it is convenient to use the scalar thrust density provided by the engine $t = T/V_{BFM}$ as the BFM design variable. This parametrization is depicted in figure 6.

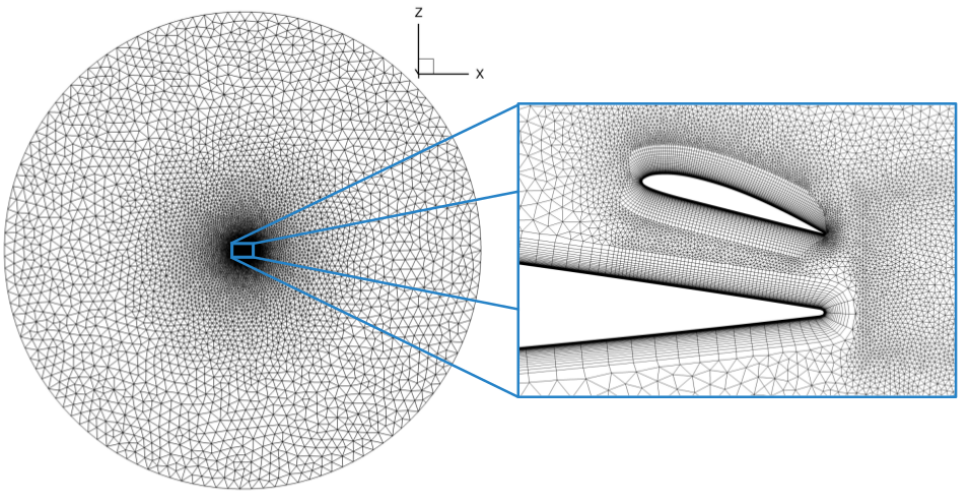

Figure 4: Bi-dimensional wing section mesh geometry

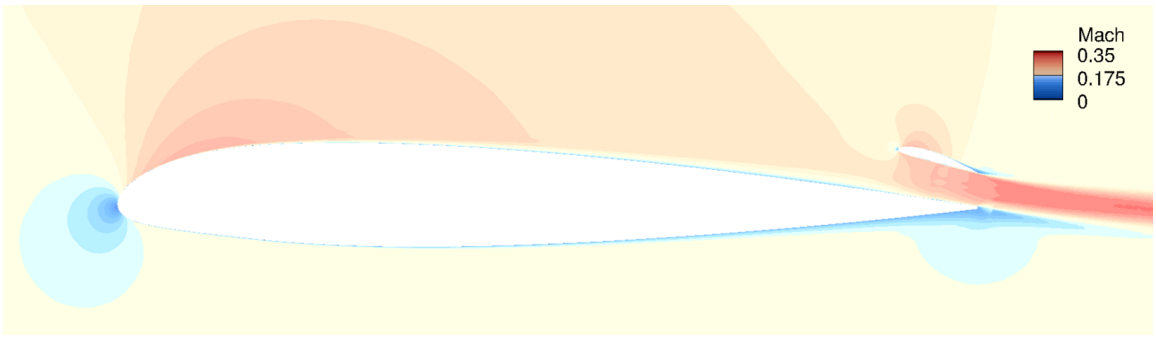

(a) Mach flow field around the wing section, at selected flight conditions

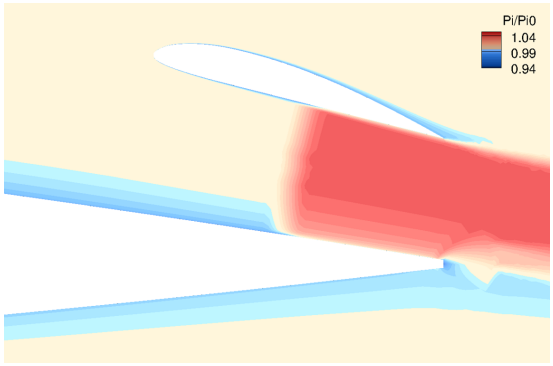

(b) Total pressure contours, divided by the upstream total pressure

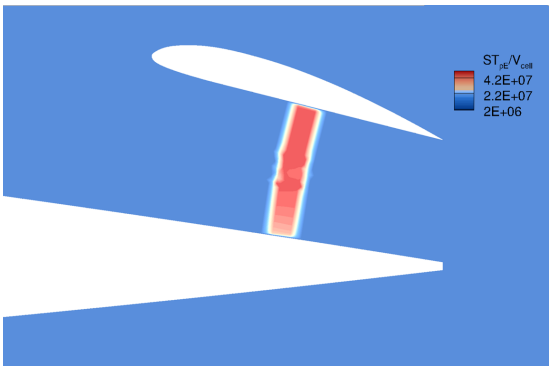

(c) BFM volume energy source term in the forcing zone

Figure 5: Mach and pressure stagnation contours around the wing section geometry, featuring a BFM forcing between the airfoil and the engine nacelle

3.2 Mesh sensitivities computation methodology and gradients validation

The adjoint system is solved in the modernized *elsA* module using an iterative Krylov algorithm with a 10^{-5} tolerance on the residual of the linear equation. However, this module cannot yet assemble the partial derivatives of $\mathcal{J}$ and $\tilde{R}$ with respect to the mesh coordinates X.

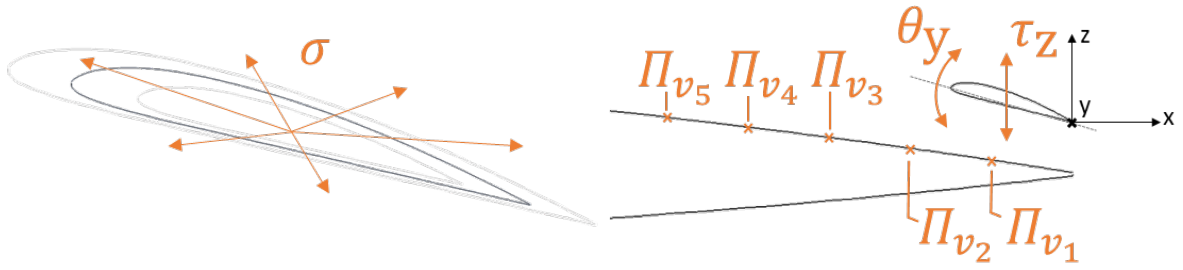

Figure 6: Parametrization chosen for the test case geometry

Therefore, a methodology has been implemented to assemble the sensitivities of $\mathcal{J}$ with respect to the shape variables, using the solution vector $\tilde{\Lambda}$ of the ABFM adjoint equations given in (5). This methodology, illustrated in figure 7, consists of producing for each shape variable α two deformed meshes $X + \Delta X$ and $X - \Delta X$, interpolating the primal flow solution W_{primal} on those and measure the QoI and residuals variations, respectively denoted $\Delta\mathcal{J}$ and $\Delta\tilde{R}$. The mesh sensitivities can then be assembled and added to the BFM sensitivities to obtain the full gradient. On the other hand, modifications were added to the modernized *elsA* module in order to assemble the partial derivatives of $\mathcal{J}$ with respect to the BFM variables β.

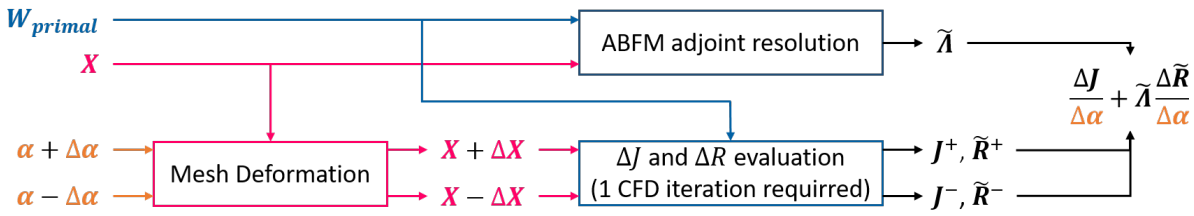

Figure 7: Methodology to compute the sensitivities of the QoI $\mathcal{J}$ with respect to the shape parameters

Adjoint gradient validation against finite difference estimation is shown here for the Π_{v_1} to Π_{v_5} shape parameters, and for the scalar thrust density t BFM parameter. For the first five parameters, only the mesh sensitivities contributes to the gradient, while for the thrust density, only the direct ABFM sensitivities contributes to it. We consider two different QoIs, the pressure drag coefficient $\mathcal{F}_{C_{D_p}}$ and the power transmitted by the engine to the flow $\mathcal{F}_{POW}$ presented in (12). We compare the obtained gradients with FD computations. FD runs show a similar residual convergence than the primal computation $\tilde{R}_\rho \approx 10^{-7}$, and a FD step study on the Π_{v_4} parameter has shown that gradient convergence is obtained as of a relative step $\delta_{FD} = 10^{-3}$. Gradient comparison against the FD estimations is shown in figure 8. Gradients have been reduced to dimensionless numbers using the QoI primal evaluation and the associated reference parameter κ value as well:

$$\nabla_{adim}\mathcal{F}(\kappa) = \nabla\mathcal{F}(\kappa) \cdot (\kappa/\mathcal{F}_{primal}) \ . \tag{17}$$

We can see a very good agreement between the adjoint and the FD results, except for the Π_{v_5} parameter, for which the relative error reaches about 26.5% of $\nabla\mathcal{F}_{C_{D_p}}(\Pi_{v_5})$ and 16% of $\nabla\mathcal{F}_{POW}(\Pi_{v_5})$. Further studies, with better FD convergence and maybe finer FD relative steps - in the validation methodology as well as in the mesh sensitivities evaluation - are required to understand the origin of this notable error for this parameter. The relative errors for the other parameters are all inferior to 1.2% for $\mathcal{F}_{C_{D_p}}$ and to 3.5% for $\mathcal{F}_{POW}$. For the BFM parameter t,

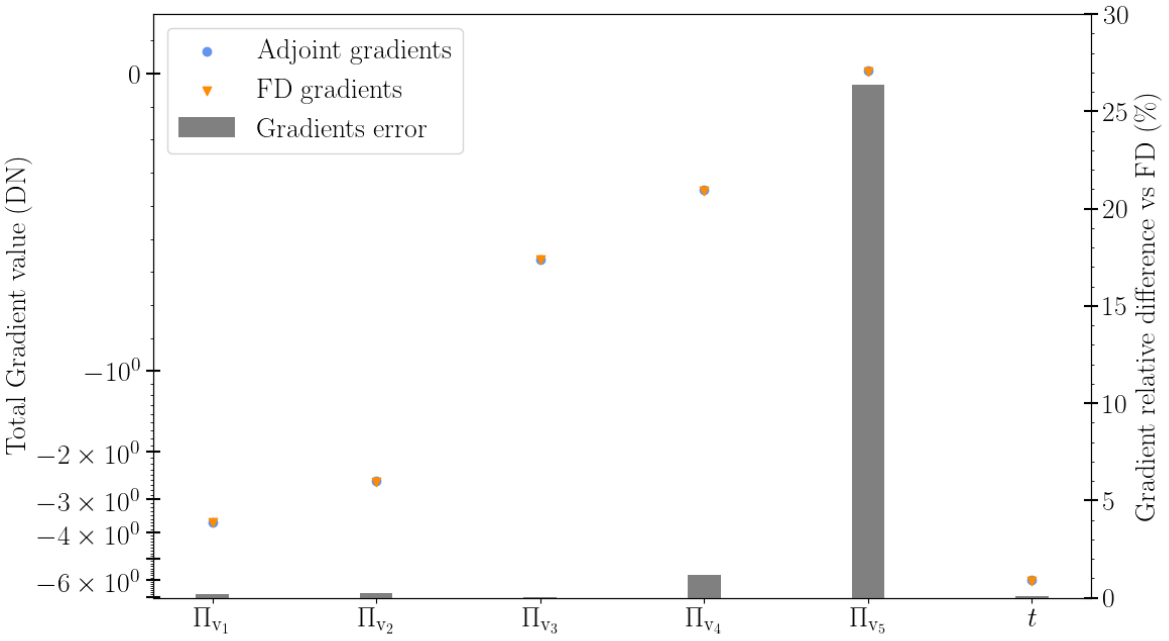

(a) Gradients validation for $\mathcal{F}_{C_{D_p}}$

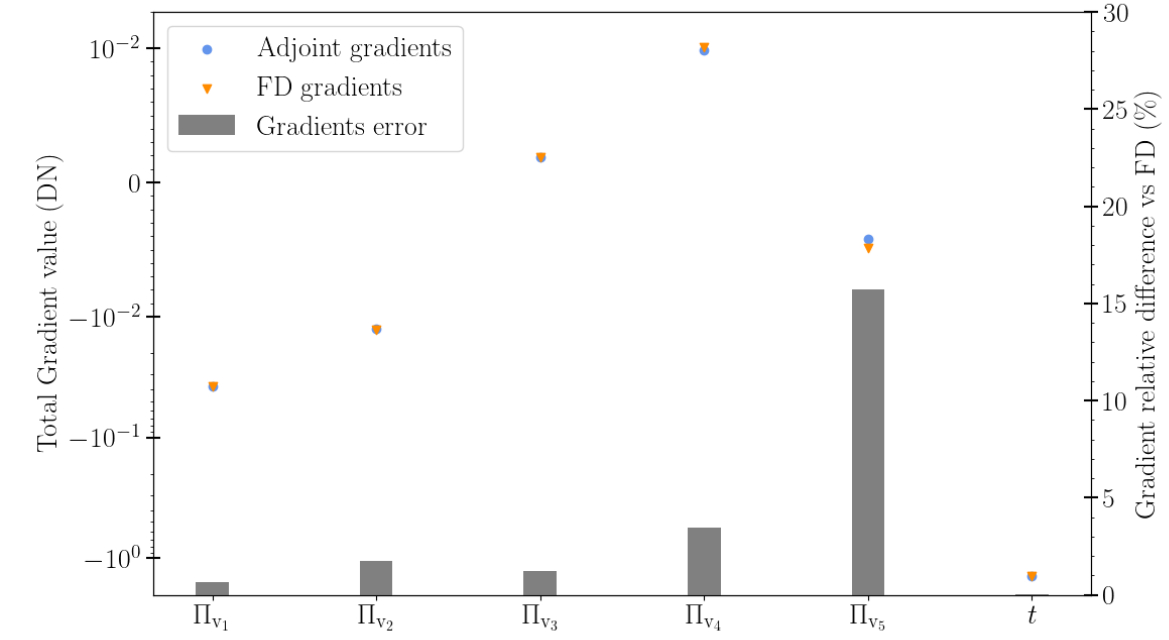

(b) Gradients validation for $\mathcal{F}_{POW}$

Figure 8: Gradient comparison between the adjoint and the FD results. FD are computed using a $\delta_{FD} = 10^{-3}$ relative step

the respective errors are $9 \cdot 10^{-2}\%$ and $6 \cdot 10^{-3}\%$, validating the ABFM implementation for this model.

3.3 Comparison of sensitivities with and without ABFM

In order to highlight the ABFM contribution to the adjoint fields and to the shape gradients, we compute the derivatives of $\mathcal{F}_{C_{D_p}}$ on the same primal solution, but removing the ABFM contribution to the adjoint equations. The purpose is to assess the error induced on the adjoint fields - and by consequences on the gradients - if one must compute the sensitivities of a given QoI using the adjoint methodology, on a coupled configuration modeled using BFM, but lacking the ABFM contribution. The classical CFD adjoint system is thus solved, its solution is denoted Λ. We then compare the resulting non-dimensional gradients for the shape parameters Π_{v_1} to Π_{v_5} in figure 9. We can see that, particularly for the shape variables parametrizing the NACA suction side in the engine vicinity, a gradient difference superior to 10% and up to 15% is obtained. Such gradient modification will most certainly alter the optimized geometry reached by the optimizer, when compared to an optimization conducted without the engine sensitivities taken into account. However, considering the significant error on $\nabla\mathcal{F}_{C_{D_p}}(\Pi_{\mathrm{v}_5})$ in the previous section, it is not possible to distinguish the ABFM contribution from the numerical error. Therefore, the important difference of about -25% observed for this parameter must be considered with precautions. In future studies, the body-force contribution to the adjoint fields will be studied in details to estimate the amplitude and the scope of the ABFM contribution.

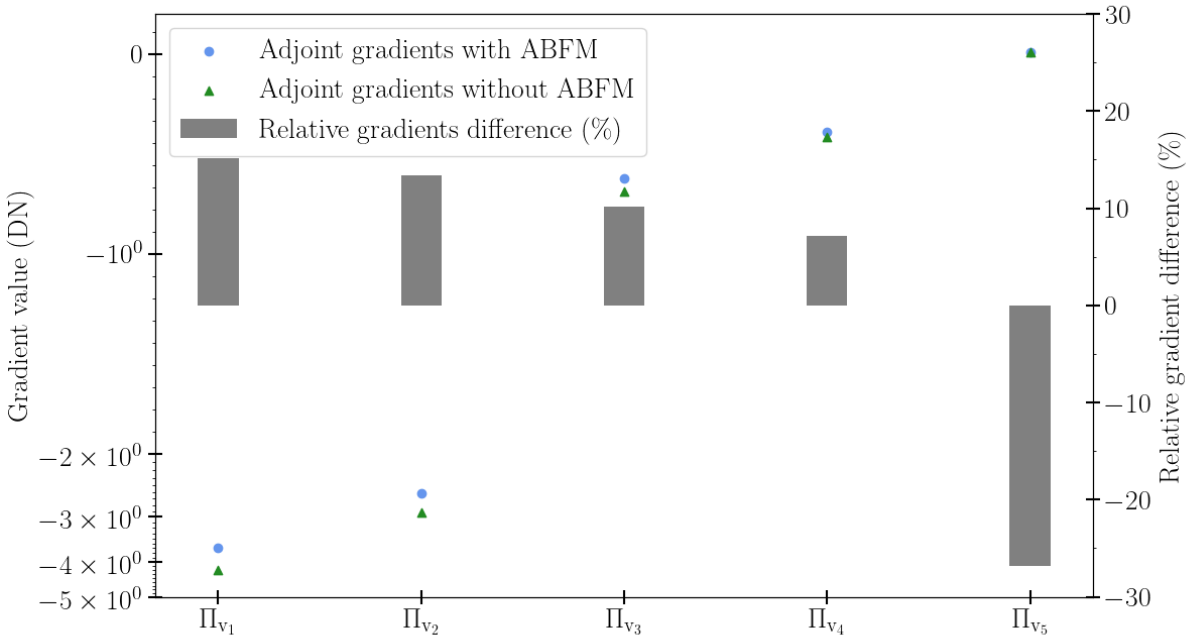

Figure 9: Gradient comparison and relative differences between adjoint computations with and without ABFM

4 A FIRST AERO-PROPULSIVE OPTIMIZATION USING THE ABFM

In this section we undertake a first optimization using the adjoint formulation of a body-force model. This first optimization, conducted on the airfoil section presented in the previous section, is undertaken by minimizing the fan power consumption $\mathcal{F}_{POW}$, considering a limited number of shape and BFM parameters - the parameters τ_z, θ_y and σ controlling the nacelle position and size, and the body-force scalar thrust density t - for which the favorable direction is known. Indeed, it is expected for the engine section to increase, and the thrust density to decrease. This behavior is comparable to the reduction of both the fan pressure ratio and the fan consumption observed when the By-Pass Ratio of a turbofan is increased. We consider the longitudinal and vertical equilibrium functions, respectively denoted $\mathcal{F}_{F_x}$ and $\mathcal{F}_{F_z}$, to ensure the aircraft operation point remains unchanged during the optimization process. $\mathcal{F}_{F_x}$ and $\mathcal{F}_{F_z}$ are built upon the drag and lift coefficients $\mathcal{F}_{C_{D_p}}$ and $\mathcal{F}_{C_{L_p}}$, and the body force momentum source term integrals $\mathcal{F}_{BFM_x}$ and $\mathcal{F}_{BFM_z}$, which are respectively given by:

$$\mathcal{F}_{BFM_x} = \iiint_{V_{BFM}} \overrightarrow{S_{\rho\vec{v}}}.\overrightarrow{e_x} dV \,, \tag{18}$$

$$\text{and } \mathcal{F}_{BFM_z} = \iiint_{V_{BFM}} \overrightarrow{S_{\rho\vec{v}}}.\overrightarrow{e_z} dV \,. \tag{19}$$

Considering a flow incidence angle ψ, $\mathcal{F}_{F_x}$ and $\mathcal{F}_{F_z}$ respectively reads :

$$\mathcal{F}_{F_x} = \mathcal{F}_{C_{D_p}} + \left[\cos(\psi)\mathcal{F}_{BFM_x} + \sin(\psi)\mathcal{F}_{BFM_z}\right](-1) \,, \tag{20}$$

$$\text{and } \mathcal{F}_{F_z} = \mathcal{F}_{C_{L_p}} + \left[-\sin(\psi)\mathcal{F}_{BFM_x} + \cos(\psi)\mathcal{F}_{BFM_z}\right](-1) \,, \tag{21}$$

since the resultant applied by the body-force on the aircraft is the opposite of the resultant computed through the momentum source terms integration. As the aircraft wing section must compensate the drag of aircraft systems not modeled here - e.g. the fuselage carrying passengers - the minimal longitudinal force amplitude required is different from 0. Because a net thrust is necessary, featuring a negative value in the chosen coordinates system, a maximum inequality constraint is imposed on the optimizer to ensure the optimized wing section provides at least the same amount of net thrust than the baseline configuration:

$$\mathcal{F}_{F_x} \leq \mathcal{F}_{F_x\,\text{baseline}} < 0 \,. \tag{22}$$

Since the vertical equilibrium must remain unchanged, two inquality constraints are imposed on the optimizer to ensure the $\mathcal{F}_{F_z}$ variation of the optimized configuration with respect to the baseline remains below 1% of its baseline value:

$$0.99\mathcal{F}_{F_z\,\text{baseline}} \leq \mathcal{F}_{F_z} \leq 1.1\mathcal{F}_{F_z\,\text{baseline}} \,. \tag{23}$$

The baseline wing section configuration features a net thrust $\mathcal{F}_{F_x\,\text{baseline}} = -2.05 \cdot 10^2\ N$ and a lift coefficient $\mathcal{F}_{C_{L_p}\,\text{baseline}} = 0.6$. The QoIs and their gradients are reduced to dimensionless numbers to help the optimizer, by the same process than previously presented in eq. 17, using the design variables and QoIs baseline values. The design variables are also reduced to dimensionless numbers. τ_z is divided by the baseline engine width $\tau_{z\text{baseline}} \approx 0.05 c_{\text{NACA}}$, and θ_y by the baseline Clark-Y angle $\theta_{y\text{baseline}} \approx 15.5\,\text{deg}$. Finally, the scalar thrust density is divided by the baseline value $t_{\text{baseline}} = 5.3 \cdot 10^5\ N.m^{-3}$ as well. Non-dimensional QoIs and variables are denoted with a suffix $_a$.

We use the optimization framework pyOpt [29] and its SLSQP optimizer implementation. The gradient values are provided to the optimizer using the new *elsA*-BACARDI ABFM capacities previously validated. Once fully reduced in non-dimensional form, the optimization can be summarized as follow:

$$\begin{aligned}
\text{minimize} \quad & \mathcal{F}_{POW\,a} \\
\text{subject to } \tau_{z a} \quad & \in \quad [-0.15\ ;\ 0.3] \\
\sigma_a \quad & \in \quad [0.8\ ;\ 1.2] \\
\theta_{y a} \quad & \in \quad [-0.13\ ;\ 0.13] \\
t_a \quad & \in \quad [-\infty\ ;\ \infty] \\
\mathcal{F}_{F_x a} \quad & \leq \quad -1.0 \\
\mathcal{F}_{F_z a} \quad & \leq \quad 1.01 \\
-\mathcal{F}_{F_z a} \quad & \leq \quad -0.99 \\
\text{regarding} \quad & \quad \tau_{z a},\ \sigma_a,\ \theta_{y a},\ t_a
\end{aligned}$$

The design variables and QoI evolution throughout the optimization process are drawn in figure 10. We can see that 8 QoIs evaluations are enough to reach the optimal design, due to the simplicity of the problem and the small size of the design space. The QoI gradient evaluations are not shown here, but 6 of them were required to reach the optimized configuration.

As expected, τ_z reaches the maximum value allowed and both the nacelle size σ and the scalar thrust density t are reduced, respectively by 10.9% and 21.1%. A very small decrease of the Clark-Y angle is also observed, by about $-1.1°$. This optimized configuration features a power fan consumption reduction of $\Delta\mathcal{F}_{POW\,a} = -6.1\%$ compared to the baseline. We can also observe that the constraints are respected, reaching the minimal $|\mathcal{F}_{F_x}|$ amplitude and the minimal $\mathcal{F}_{F_z}$ allowed. This is expected since minimizing the net wing section thrust and lift coefficient helps minimizing the engine power consumption.

In figure 11, we present for the optimized configuration the same flow field analysis than the one conducted on the baseline geometry (see figure 5). In addition, in figure 11b, a sketch of the Clark-Y re-sizing and position change is proposed to illustrate the amplitude of each transformation. The baseline geometry is drawn in black, the optimized one in red. For instance, the Clark-Y size change can be illustrated by the change of its chord length. Comparing figures 11a and 5a, we observe a smaller flow acceleration across the engine for the optimized configuration. Similarly and as expected, the optimized design show a smaller total pressure rise across the engine than the baseline (see figures 11c and 5b). Therefore, less kinetic energy is wasted in the engine jet flow per unit of volume for the optimized design. However, the enlargement of the engine has increased the mass-flow rate and the width of the jet wash. Therefore, an exergy analysis [30] would be required to precisely assess the aeropropulsive benefits.

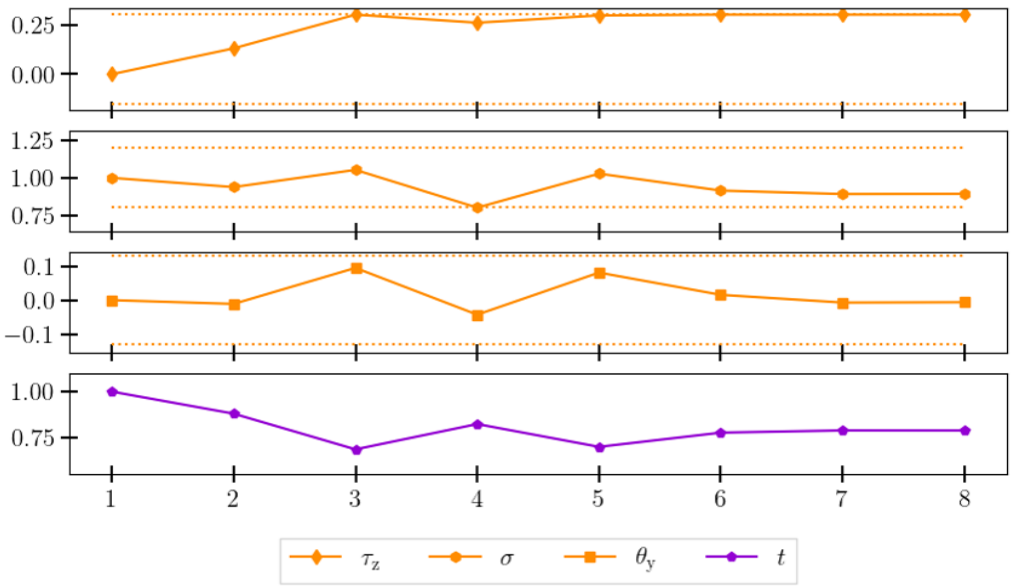

(a) Design variables non-dimensional values for during the optimization iterations. The bounds of the design variables are drawn in dotted lines.

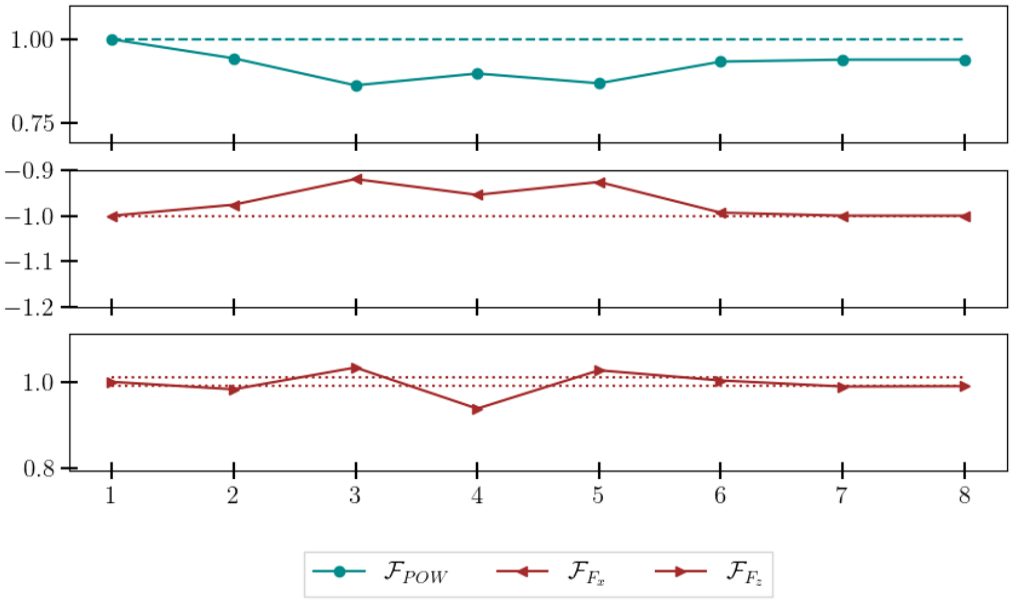

(b) Objective function (in blue) and constraints (in red) non-dimensional values during the optimization iterations. Constraints bounds are represented in dotted lines, while the initial objective function value is drawn using dashed lines.

Figure 10: Optimization convergence history for both the design variables (top) and the QoIs (bottom).

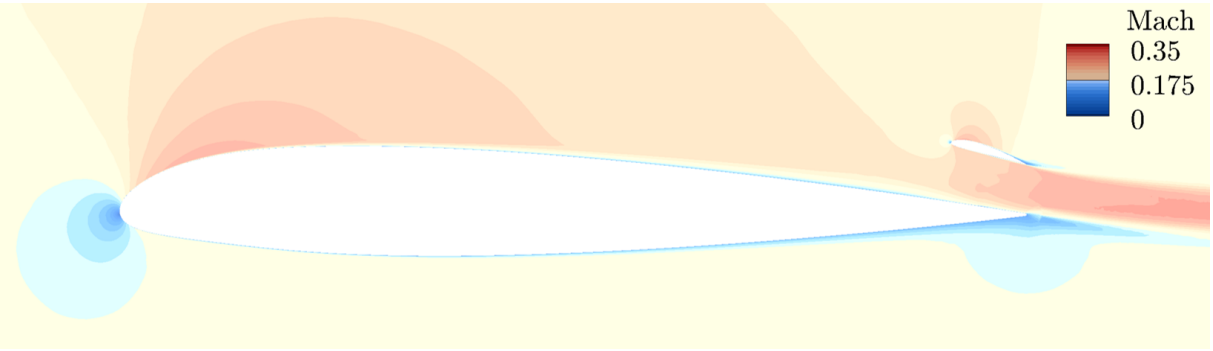

(a) Mach flow field around the optimized geometry, at selected flight conditions.

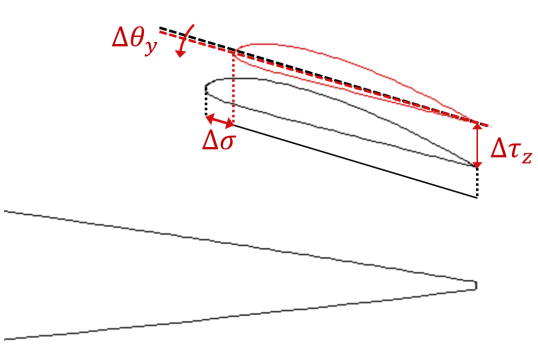

(b) Sketch of the Clark-Y position and size change for the optimized configuration (in red) with respect to the baseline (in black).

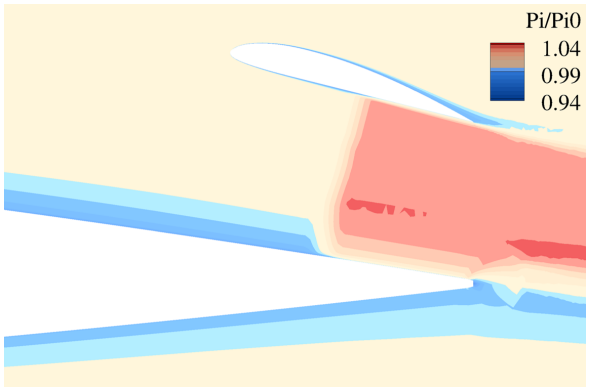

(c) Total pressure contours around the optimized configuration, divided by the upstream total pressure.

Figure 11: Flow field analysis of the optimized wing section (top and bottom right) and sketch of the shape variation between the baseline and the optimized configurations (bottom left).

CONCLUSIONS AND FUTURE WORK

The current work has introduced the Adjoint Body-Force equations and proposed an efficient methodology to implement it. In section 2, the ABFM implementation has been successfully undertaken in the *elsA* framework, for a simplified explicit BFM model. In section 3, a body-force model of interest for the conceptual design stages has been implemented, as well as its adjoint formulation. The gradients involving direct or indirect ABFM sensitivities have been validated against finite-differences. Then, we have highlighted the strong influence of the ABFM sensitivities on the airframe shape gradients, with a relative differences of about 10%, even far from the BFM forcing zone. Such result shows that neglecting the propulsive sensibilities during an aero-propulsive optimization would strongly affect the optimal solution, since the optimizer lacks important information on the aero-propulsive coupling phenomena and trade-off balance. Finally, in section 4, we have presented and validated the ABFM optimization framework set up, using an optimization test-case for which the leading-order behavior can be deduced based on simple physical considerations. The results obtained for this test-case are consistent with the expectations. Thus, the ABFM optimization framework can now be used to conduct more complex optimization, featuring a greater number of design variables.

These results strengthen the idea that the adjoint body-force is a promising tool to undertake aero-propulsive optimization at a reasonable computational cost, on configurations featuring a strong coupling between the engine and the airframe aerodynamics. However, as the other studies available in the literature [12, 14, 13, 8], blade shape parameters are not considered in the engine model used for this study. Therefore the effects of the fan geometry on the distortion dampening and transfer across the engine [6] cannot be assessed using the 'T-spread' model. In order to consider the engine aerodynamic response to distortions and its dependencies on the blade shape parameters, a three dimensional propulsive model, with higher modeling fidelity and directly coupled to the local flow variables, is needed. The BFM model proposed by Hall [20] in 2015, latter modified by Thollet [15] and Godard [6], is adapted to such studies.

In our future work, we will conduct more complex optimization on the bi-dimensional wing section geometry, with a larger set of design variables. Then, we will evaluate the Hall model capabilities to optimize axisymmetric and three-dimensional airframe configurations, while taking into account the sensitivities due to the engine system thanks to the ABFM. Later, we will try to undertake a simultaneous optimization of both the engine and the airframe designs, by the use of the Hall ABFM implementation.

ACKNOWLEDGMENTS

This work was partially founded by the Clean Sky 2 Joint Undertaking project, granted by the European Union. The authors would like to acknowledge Carlos Díaz Durán for his previous studies on the wing section geometry. These studies have provided the shape parametrization used in this work and reference results.

REFERENCES

[1] G. G. Fleming, "Environmental trends in aviation to 2050," tech. rep., ICAO, 2016.

[2] I. A. T. Association, "Working Towards Ambitious Targets."

[3] M. Borel and B. Vinstock, "Aviation & changement climatique," tech. rep., Direction Générale de l'Aviation Civile, Mar. 2018.

[4] S. Delbecq, J. Fontane, N. Gourdain, H. Mugnier, T. Planès, and F. Simatos, "Aviation and Climate : a literature review," Tech. Rep. 1.1, ISAE-SUPAERO, Toulouse, France, 2022.

[5] A. Peters, Z. S. Spakovszky, B. Rose, and W. K. Lord, "Ultra-Short Nacelles for Low Fan Pressure Ratio Propulsors," *American Society of Mechanical Engineers*, p. 15, 2014.

[6] B. Godard, *Étude et méthodologies de simulation de doublet entrée d'air - soufflante pour la conception de turbofan de nouvelle génération*. PhD Thesis, Université de Toulouse, 2018.

[7] P. Schmollgruber, D. Donjat, M. Ridel, I. Cafarelli, O. Atinault, C. François, and B. Paluch, "Multidisciplinary Design and performance of the ONERA Hybrid Electric Distributed Propulsion concept (DRAGON)," in *AIAA Scitech 2020 Forum*, (Orlando, FL), American Institute of Aeronautics and Astronautics, Jan. 2020.

[8] J. S. Gray, C. A. Mader, G. K. W. Kenway, and J. R. R. A. Martins, "Coupled Aeropropulsive Optimization of a Three-Dimensional Boundary-Layer Ingestion Propulsor Considering Inlet Distortion," *Journal of Aircraft*, vol. 57, pp. 1014–1025, Nov. 2020.

[9] Q. Bennehard, "Aerodynamic shape optimization of a short medium range blended wing body aircraft," in *56th 3AF International Conference AERO2022*, (Toulouse, France), May 2022.

[10] M. Carini, C. Blondeau, N. Fabbiane, M. Meheut, M. Abu-Zurayk, J. M. Feldwisch, C. Ilic, and A. Merle, "Towards industrial aero-structural aircraft optimization via coupled-adjoint derivatives," in *AIAA AVIATION 2021 FORUM*, (VIRTUAL EVENT), American Institute of Aeronautics and Astronautics, Aug. 2021.

[11] G. K. W. Kenway and J. R. R. A. Martins, "Multipoint High-Fidelity Aerostructural Optimization of a Transport Aircraft Configuration," *Journal of Aircraft*, vol. 51, pp. 144–160, Jan. 2014.

[12] G. K. Kenway and C. C. Kiris, "Aerodynamic Shape Optimization of the STARC-ABL Concept for Minimal Inlet Distortion," in *2018 AIAA/ASCE/AHS/ASC Structures, Structural Dynamics, and Materials Conference*, (Kissimmee, Florida), American Institute of Aeronautics and Astronautics, Jan. 2018.

[13] J. S. Gray and J. R. R. A. Martins, "Coupled aeropropulsive design optimisation of a boundary-layer ingestion propulsor," *The Aeronautical Journal*, vol. 123, pp. 121–137, Jan. 2019.

[14] I. Ordaz, S. K. Rallabhandi, E. J. Nielsen, and B. Diskin, "Mitigation of Engine Inlet Distortion through Adjoint-Based Design," in *35th AIAA Applied Aerodynamics Conference*, (Denver, Colorado), American Institute of Aeronautics and Astronautics, June 2017.

[15] W. Thollet, *Modélisations simplifiées de turbomachines pour l'analyse par la simulation des installations motrices complexes d'avions/Body force modeling of fan-airframe interactions*. PhD Thesis, Université de Toulouse, July 2017.

[16] B. Godard, E. De Jaeghere, and N. Gourdain, "Efficient Design Investigation of a Turbofan in Distorted Inlet Conditions," in *Volume 2A: Turbomachinery*, (Phoenix, Arizona, USA), p. V02AT39A011, American Society of Mechanical Engineers, June 2019.

[17] W. Thollet, G. Dufour, X. Carbonneau, and F. Blanc, "Assessment of body-force methodologies for the analysis of intake–fan aerodynamic interactions," *American Society of Mechanical Engineers*, p. 9, 2016.

[18] B. Godard, N. Ben Nasr, R. Barrier, J. Marty, N. Gourdain, and E. De Jaeghere, "Methodologies for Turbofan Inlet Aerodynamics Prediction," in *35th AIAA Applied Aerodynamics Conference*, (Denver, Colorado), American Institute of Aeronautics and Astronautics, June 2017.

[19] S. Pazireh, *Body Force Modeling of Axial Turbomachines Without Calibration*. PhD Thesis, University of Windsor, Ontario, Canada, Mar. 2021.

[20] D. K. Hall, *Analysis of civil aircraft propulsors with boundary layer ingestion*. PhD Thesis, MIT, 2015.

[21] J. Peter, *Contributions to discrete adjoint method in aerodynamics for shape optimization and goal-oriented mesh adaptation*. HDR Thesis, Université de Nantes, Sept. 2020.

[22] G. Carrier, D. Destarac, A. Dumont, M. Meheut, I. Salah El Din, J. Peter, S. Ben Khelil, J. Brezillon, and M. Pestana, "Gradient-Based Aerodynamic Optimization with the elsA Software," in *52nd Aerospace Sciences Meeting*, (National Harbor, Maryland), American Institute of Aeronautics and Astronautics, Jan. 2014.

[23] J. Peter, F. Renac, A. Dumont, and M. Méheut, "Discrete adjoint method for shape optimization and mesh adaptation in the elsA code. Status and challenges," in *50h 3AF International Conference on Applied Aerodynamics*, (Toulouse, France), p. 14, Apr. 2015.

[24] A. P. Kottapalli, "Development of a Body Force Model for Centrifugal Compressors," Master's thesis, Massachusetts Institute of Technology, Aug. 2013.

[25] L. Hascoet and V. Pascual, "The Tapenade automatic differentiation tool: Principles, model, and specification," *ACM Transactions on Mathematical Software*, vol. 39, pp. 1–43, Apr. 2013.

[26] B. Maugars, S. Bourasseau, C. Content, B. Michel, B. Berthoul, J. N. Ramirez, P. Raud, and L. Hascoët, "Algorithmic Differentiation for an efficient CFD solver," in *ECCOMAS 2022 - 8th European Congress on Computational Methods in Applied Sciences and Engineering*, (Oslo, Norway), p. 22, June 2022.

[27] L. Cambier, S. Heib, and S. Plot, "The Onera *elsA* CFD software: input from research and feedback from industry," *Mechanics & Industry*, vol. 14, no. 3, pp. 159–174, 2013.

[28] B. Kulfan, "A Universal Parametric Geometry Representation Method - "CST"," in *45th AIAA Aerospace Sciences Meeting and Exhibit*, (Reno, Nevada), American Institute of Aeronautics and Astronautics, Jan. 2007.

[29] R. E. Perez, P. W. Jansen, and J. R. R. A. Martins, "pyOpt: A Python-based object-oriented framework for nonlinear constrained optimization," *Structures and Multidisciplinary Optimization*, vol. 45, no. 1, pp. 101–118, 2012.

[30] A. Arntz, *Civil Aircraft Aero-thermo-propulsive Performance Assessment by an Exergy Analysis of High-fidelity CFD-RANS Flow Solutions*. PhD Thesis, Université de Lille, 2014.